First-Time Soil Moisture Retrieval Using Single-Frequency Dual-Polarization GNSS-R with Airborne GLORI Data

Xuerui Wu

Abstract*—Polarization was once overlooked in GNSS-R studies. However, in recent years, it has garnered increasing interest. This paper explores dual polarization for single-frequency data from the airborne GLORI experiment. Building on theoretical analysis, we have applied several retrieval algorithms for soil moisture estimation. Initially, only the surface reflectivity of LR and RR polarizations was examined. As additional surface parameters, such as surface roughness and vegetation, were incorporated into the algorithm, the retrieval accuracy, as indicated by RMSE, improved from around 0.07 to 0.03. The accuracy retrieved by RR polarization appears slightly better than that of LR polarization. However, when both dual polarizations were considered, the retrieval accuracy matched that of using only one polarization. When surface roughness, LAI, and incidence angle are taken into account, the retrieval accuracy, as indicated by RMSE, is 0.0344. This suggests that dual polarization holds great potential for soil moisture estimation. GLORI data is the first publicly available dual polarization GNSS-R data that includes both coherent and noncoherent scattering. This paper also discusses the noncoherent scattering properties of LR and RR polarizations. In the realm of coherent scattering, it is observed that the scattering properties at LR polarization exceed those at RR polarization. However, this trend reverses for noncoherent scattering, wherein the scattering properties at LR polarization are diminished compared to those at RR polarization for corresponding land surface types. The analysis of dual polarizations data will benefit future data mining for more accurate soil moisture retrieval and the design of future polarization GNSS-R payloads. While the retrieval accuracy with the consideration of noncoherent scattering properties indicates that not only coherent scattering but also noncoherent scattering should be included in future GNSS-R data sets, they are comparable for future soil moisture retrieval algorithms.

***Index Terms*—polarization, coherent scattering, non-coherent scattering, GNSS-R, soil moisture, surface roughness, vegetation.**

I. INTRODUCTION

GNSS-R has emerged as one of the most crucial and pioneering remote sensing techniques over the past three decades [1], [2], [3], [4], [5]. With an increasing number of in-orbit GNSS satellites, the availability of incidence signal sources has also grown. This expansion is expected to enhance the network of GNSS-R missions, offering significant potential to improve the spatial and temporal resolutions of GNSS-R data.

The United Kingdom Disaster Monitoring Constellation (UK-DMC) marked the inception of GNSS-R missions used to showcase the potential of space-borne GNSS-R missions for Earth remote sensing [6]. Surrey Satellite Technology Ltd (SSTL), the designer of UK-DMC, subsequently launched the UK TDS-1 into space. While the primary objective of TDS-1 was to detect ocean surface parameters, it also collected reflected signals from the land surface, demonstrating its significant potential for detecting Earth surface geophysical parameters [7], [8]. In December 2012, NASA's CYGNSS, comprising eight small GNSS-R satellites, was launched with a spatial coverage of ±38° [9]. Initially focused on detecting cyclone status in pan-tropical regions, researchers discovered that the reflected signals from the land surface could be utilized to detect near-surface soil moisture [10], [11], [12], [13], [14], [15], forest biomass [16], [17], [18], flood inundation [19], [20], and near-surface soil freeze/thaw status [21], [22], [23], [24]. Subsequently, other GNSS-R missions such as WINSAT-1R, Bufeng 1-A/B, UK DoT-1, and FSSCat have been successively launched. In July 2021, China's FengYun 3E was launched, featuring the GNOS-R as one of its eleven payloads [25]. This marked the first global coverage GNSS-R payload, showcasing its capability not only in detecting ocean surface parameters, but also in retrieving soil moisture and detecting near-surface freeze/thaw conditions [26], [27]. Additionally, in 2024, the HydroGNSS is scheduled for launch. It's noteworthy that all GNSS-R payloads utilize LHCP (Left Hand Circular Polarization) antennas, with the exception of HydroGNSS, which will feature two antennas—one LHCP and the other RHCP (Right Hand Circular Polarization) [28]. Researchers anticipate using dual polarization to mitigate the impacts of surface roughness and vegetation effects, thereby enhancing the accuracy of soil moisture retrieval.

Based on the aforementioned GNSS-R developments, it is evident that polarization will be a pivotal feature in future GNSS-R advancements [29], [30].

As we known, polarization determines the direction characteristics of the electric field vector in electromagnetic waves, and different polarization methods endow electromagnetic waves with unique properties and applications. Linearly polarized electromagnetic waves perform excellently

This work was supported in part by the National Natural Science Foundation of China (No. 42061057).and Key Laboratory of Satellite Navigation Technology. *(Corresponding author: Xuerui Wu).*

Xuerui Wu is with Shanghai Astronomical Observatory, Chinese Academy of Sciences, Shanghai 200030, China (e-mail: xrwu@shao.ac.cn).

in communication systems and radars; in the Beidou/GNSS field, they are widely used in satellite communication and radio frequency identification, which can reduce the multipath effect and improve signal reliability and anti-interference ability. In GNSS - R remote sensing research, polarization is also crucial. The signals usually emitted by GNSS satellites are right-hand circularly polarized, and the polarization state changes after being reflected from the Earth's surface, containing rich information on the characteristics of the Earth's surface. For example, different types of surfaces have large differences in the reflection characteristics of polarized signals. Information coverage such as surface roughness, vegetation height, and soil moisture can be obtained by analyzing the polarization changes of the reflected signals. It can be seen from the development of GNSS-R that the attention to its polarization characteristics is relatively weak. However, soil moisture can be estimated more accurately by comparing the parameters of the reflected signals under different polarization methods. Polarization can also distinguish different scattering mechanisms in GNSS - R remote sensing. By studying the changes in the polarization state, the signal scattering process can be better understood, providing a basis for establishing a more accurate scattering model of the Earth's surface.

In GNSS-R soil moisture remote sensing studies, specular reflection signals are frequently employed for inversion. Specifically, the effective reflectivity is identified within the DDM waveform, which is regarded as the specular scattering from the mirror reflection point and is subsequently utilized for inversion. However, on complex terrestrial surfaces, the direct signal incident from the navigation satellite is reflected by the ground, scattering energy in all directions. The rougher the surface, the less energy is reflected in a specular direction, with diffuse scattering making the primary contribution. Nevertheless, research has indicated that in the process of soil moisture inversion, it is not the existing specular or backscattering energy that is optimal for inversion. Instead, employing noncoherent scattering under different observational geometries can effectively retrieve soil moisture. However, due to the initial limitations on GNSS-R observation data, effectively separating the noncoherent terms from the existing space-borne observed DDM waveform data seems to be challenging.

Therefore,it is important tol focus on the polarizations properties on GNSS-R soil moisture study and there is a need to develop retrieval algorithms for single-frequency dual polarization with the considerations of non-coherent scattering properties and its values for the final retrieval accuracy will also provided in this paper.

Due to the limited availability of spaceborne GNSS-R dual-polarization data, this paper aims to utilize airborne GNSS-R data from GLORI to conduct a preliminary study demonstrating the potential for soil moisture retrieval using dual polarizations [31]. To the best of our knowledge, GLORI represents the first instance in which a comprehensive dataset of GNSS-R observables, including reflectivity and the incoherent component relative to the total scattering signal-to-noise ratio (SNR) for copolarized (right-right) and cross-polarized (right-left) measurements, has been made accessible.

II. Theoretical Methods and Data Description

A. Dual Polarization Reflectivity

For an ideal smooth surface, reflectivity is determined by the Fresnel reflection coefficient and the polarization mode of the incident signals. The Fresnel reflection coefficients for horizontal and vertical polarizations are as follows [32]:

$$r_h = \frac{\cos\theta - \sqrt{\varepsilon_r - \sin^2\theta}}{\cos\theta + \sqrt{\varepsilon_r - \sin^2\theta}} \tag{1}$$

$$r_v = \frac{\varepsilon_r \cos\theta - \sqrt{\varepsilon_r - \sin^2\theta}}{\varepsilon_r \cos\theta + \sqrt{\varepsilon_r - \sin^2\theta}} \tag{2}$$

While is the incidence angle, is the complex dielectric constant, the subscripts and demonstrate the polarization state.

For perfectly smooth surfaces, the cross-polarization term and can be disregarded. In the case of GNSS signals, the satellite transmission signal is RHCP, which can be interpreted as a linear combination of horizontal and vertical polarization components[32].

$$r_h = \frac{\cos\theta - \sqrt{\varepsilon_r - \sin^2\theta}}{\cos\theta + \sqrt{\varepsilon_r - \sin^2\theta}} \tag{3}$$

The equations for LR polarization reflectivity, provided below, demonstrate that it is a linear combination of the Fresnel reflectivity for vertical and horizontal polarizations [32].

$$r_v = \frac{\varepsilon_r \cos\theta - \sqrt{\varepsilon_r - \sin^2\theta}}{\varepsilon_r \cos\theta + \sqrt{\varepsilon_r - \sin^2\theta}} \tag{4}$$

As for bare soil, the surface reflectivity (SR) can be demonstrated as the following [33]:

$$\Gamma_{rr} = \frac{1}{2}\left(r_{vv} + r_{hh}\right) = \frac{\left(\varepsilon_r - 1\right)^2 \sin^4\theta}{\left(\varepsilon_r \sin\theta + \sqrt{\varepsilon_r - \sin^2\theta}\right)^2 \left(\cos\theta + \sqrt{\varepsilon_r - \sin^2\theta}\right)^2} \tag{5}$$

While SR is the surface reflectivity, θ is the incidence angle, ε_r is the dielectric constant.

Meanwhile, Wu et al. have also developed random rough surface models for GNSS-R polarization study [33], [34]. For example, they proposed the LAGRS models for land surface parameters study, and one of the important components of the models is for bare soil study [35], [36]. In order to support future polarization GNSS-R payloads, random surface scattering models including RR polarization have also been proposed in their model

The scattering models in LAGRS-Soil have the ability to

calculate the scattering properties at various polarizations, as shown in Figure 1 [33]. From the figure, we can see that the scattering properties vary at different polarizations. While SR is the specular reflectivity that is encompassed within the calculation capabilities of LAGRS-Soil (BRCS). For the retrieval algorithm development in this paper, we will use the scattering properties calculated from both Equations 1-4 and the LAGRS-Soil scattering properties [33].

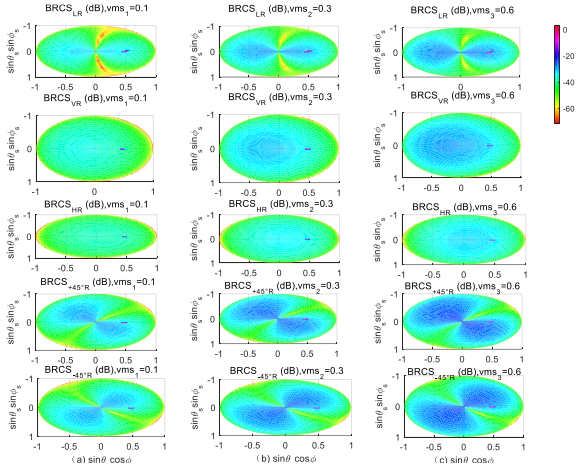

Fig. 1. Random rough surface scattering for various polarizaitons [34].BRCS is short for bistatic radar cross section. while the subscripts of LR, VR,HR, +45°R,-45°R in each rows indicate the polarziations status of LHCP received-RHCP transimitted, vertical pol received-RHCP pol transmitted, horizontal pol received-RHCP pol transmitted, +45° pol received-RHCP pol transmitted, -45° pol received-RHCP pol transmitted. vsm is short for volumetric soil moisture, the subscript 1,2,3 in each column is for the different soil moisture contents as shown in the figures. θ and φ are the indicators of incidence zenith angles and azimuth angles. θ_s and φ_s are the scattering zenith angles and azimuth angles

For surfaces covered with vegetation, the ultimate surface reflectivity should be reduced by the vegetation layer, and the corresponding equations are provided below [37].

$$SR(\theta) = \Re^2(\theta)\gamma^2 exp\left(-4k^2s^2cos^2(\theta)\right)\theta_s\varphi_s \quad (6)$$

$$\gamma = exp(-\tau * csc(\theta)) \quad (7)$$

while SR is the surface reflectivity, $\Re$ *is the Fresnel reflectivity ,* τ *is the vegetation opacity depth, k is free wavenumber, s is the rms height,* θ is the incidence angles at the specular directions.

B. Data Description

To the best of our knowledge, this marks the first instance in which a comprehensive dataset of GNSS-R observables (encompassing reflectivity, incoherent component relative to the total scattering signal-to-noise ratio (SNR) for copolarized (right-right) and cross-polarized (right-left) measurements) has been made accessible [31].

The GLORI campaigns were carried out in Catalonia, Spain, specifically over the Urgell region, which includes an agricultural area with two distinct components. The first segment relies on intensive irrigation, drawing water from the Pyrenees via the Urgell canal. The second segment comprises rain fed agriculture and grassland. The specific locations of the land cover dataset and the in situ measurement dataset are illustrated in Figure 2.

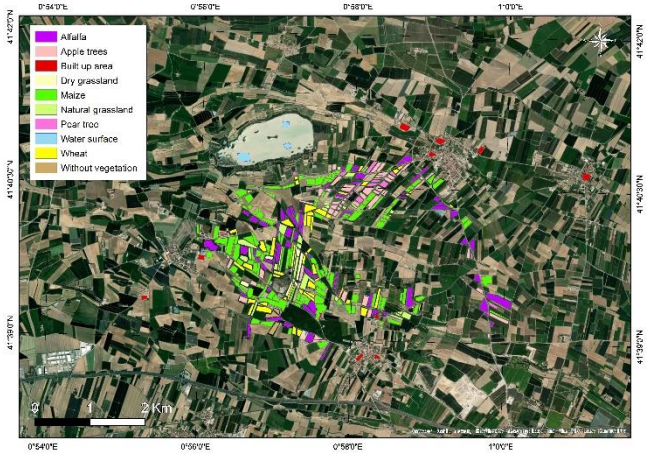

Fig. 2. Land Cover and Land Types for Airborne GLORI Experiment.

The airborne dataset was derived from raw data collected during three flights carried out using the French research ATR-42 aircraft in July 2021 (specifically, flights 45, 46, and 47, conducted on July 22nd, 27th, and 28th, respectively) over the Urgell site.

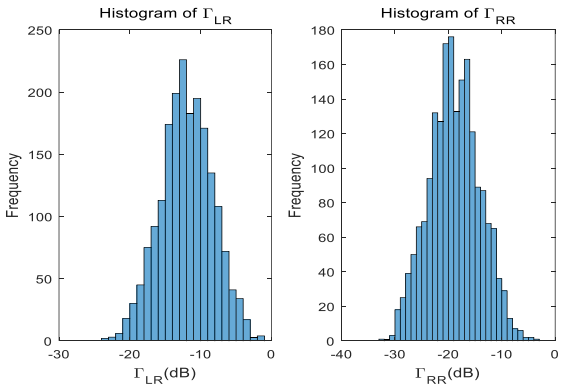

Fig. 3. Histogram of Surface Reflectivity for LR Polarization (Left) and RR Polarization (Right).

From the demonstration of Figure 3, it is evident that the surface reflectivity at LR polarization is slightly higher than that at RR polarization, with mean values of -11.98 and -18.83, respectively. The dynamic range for surface reflectivity at LR polarization and RR polarization are -21.19dB and -30.13dB, respectively. Histograms for RMS height, LAI, and soil moisture content are depicted in Figure 4. Given that RMS height is a crucial factor for soil moisture content correction and LAI offers insights into vegetation parameters, both will require correction during soil moisture retrieval. Statistical information for these three parameters is detailed in Table 1. The mean value for RMS height is 0.84 cm, with a mode value of 0.91 cm. As for LAI, the mean and mode values are 1.34 and 0.49, respectively. Both the mean and mode values for soil moisture content(smc) are 0.23.

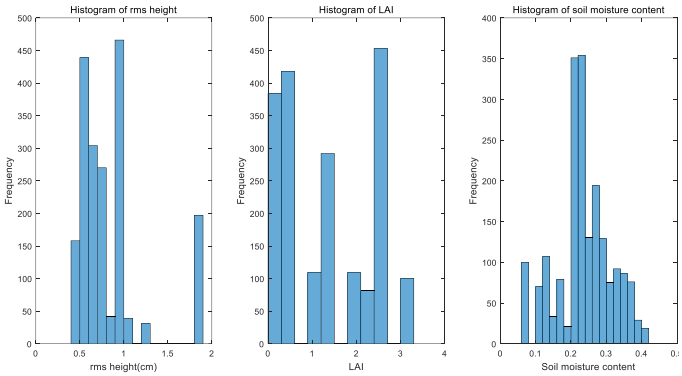

Fig. 4. Histograms for Surface Roughness (RMS Height),Vegetation Parameters (LAI), and Soil Moisture Content.

TABLE I
STATISTICAL DATA FOR SURFACE REFLECTIVITY AT LR AND RR POLARIZATIONS, SURFACE ROUGHNESS (RMS HEIGHT), VEGETATION PARAMETERS (LAI), AND SOIL MOISTURE CONTENT.

	Γ_{LR}	Γ_{RR}	RMS height(cm)	LAI	smc
Mean	-11.98	-18.83	0.84	1.34	0.23
Mode	-21.19	-30.13	0.91	0.49	0.23

III. SOIL MOISTURE RETRIEVAL

Since space-borne GNSS-R payloads are typically single-polarized, meaning that the GNSS-R receiver uses an LHCP antenna to capture Earth's surface-reflected signals, LR polarization has been used to extract geophysical parameters. Consequently, the retrieval algorithm for single-frequency single polarization is presented in this section. In the next section, the retrieval algorithm for single-frequency dual polarizations will be presented, along with a comparison between these two algorithms.

Artificial intelligence (AI) techniques offer new perspectives and solutions for addressing complex issues in the Earth system, thanks to their exceptional data processing capabilities and pattern recognition abilities. Neural networks have demonstrated remarkable capabilities in soil moisture retrieval with remote sensing data. .

In this section, ANN (Artificial Neural Networks) will be employed for the evaluations of the soil moisture retrieval algorithms and the development of ANN algorithms are based the equations provided section 2. GLORI experiment encompasses a total of three airborne flight tests, namely Flight 45, 46, and 47. The available sample numbers it obtained were 564, 622, and 760 respectively, totaling 1,946 data. When using the following ANN algorithm for learning, 100 non-repeated numbers were randomly selected from them as the test set data, and the remaining 1,846 data were used for the training set.

A. single frequency and single polarization retrieval

Equation 1-7 clearly shows that surface reflectivity is influenced by several factors, including soil moisture, surface roughness, and vegetation optical depth. These factors are crucial parameters that must be taken into account in the final retrieval. The quantitative analysis results are illustrated in the following figures.

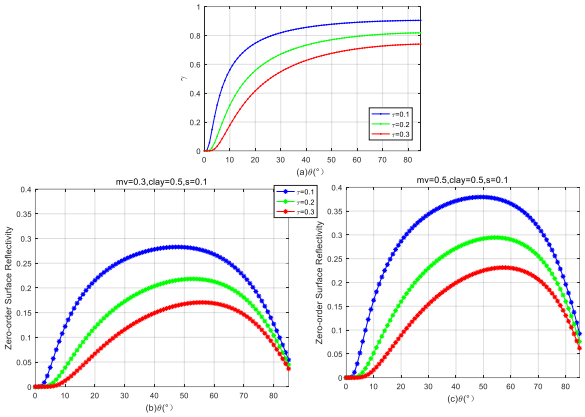

Fig. 5. theoretical simulations for attenuation factor and surface reflectivity with the zero-order model.

In the Figure 5(a) , it is evident that as the incidence angle (ranging from 0° to 30°) increases, the vegetation attenuation factor also increases. However, when the incidence angle exceeds 30°, the vegetation optical depth exhibits minimal impact on the incidence angle. Nevertheless, the effects of vegetation optical depth on the final attenuation factors are notably pronounced, with attenuation decreasing as the optical depth increases. The combined effects of soil moisture and vegetation optical depth are demonstrated in Sub figures 5(b) and 5(c). From the aforementioned simulations, it is clear that the influences of soil moisture, vegetation optical depth, and surface roughness should all be taken into consideration in the subsequent development of the retrieval algorithm.

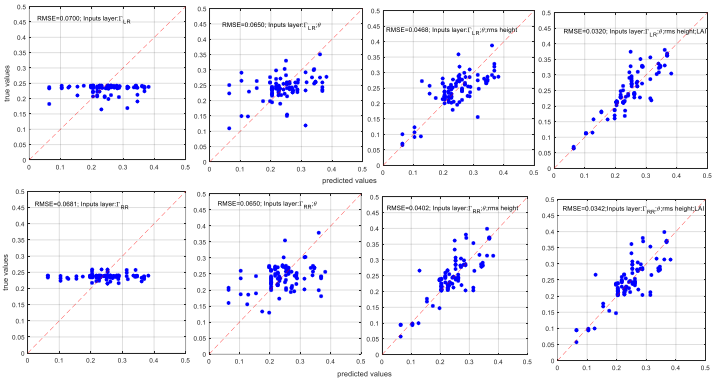

Fig. 6. single-frequency, single-polarization soil moisture retrieval using GLORI data. In the first row, the retrieval is based on the surface reflectivity of LR polarization, whereas in the second row, the retrieval is conducted using RR polarization.

Fig. 6 depicts single-frequency, single-polarization soil moisture retrieval using GLORI data. In the first row, retrieval

is performed using the surface reflectivity of LR polarization, while in the second row, retrieval is conducted using RR polarization. In the first column, only surface reflectivity information is utilized, while in the second column, incidence angle is incorporated. In the third and fourth columns, surface roughness (rms height) and vegetation parameters (LAI) are employed for the retrieval.

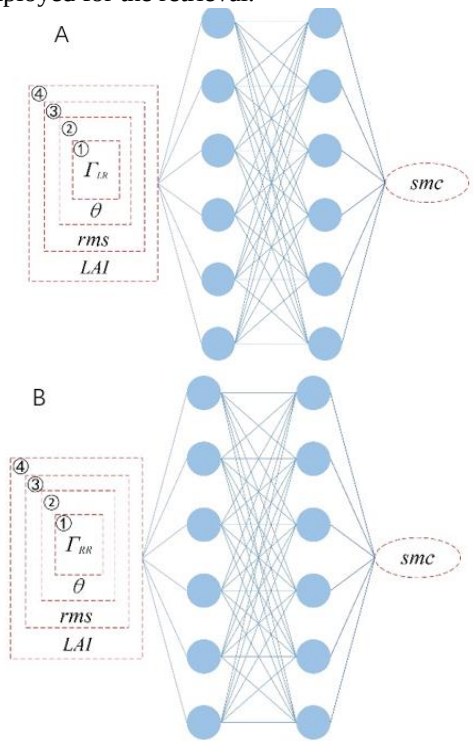

Fig. 7. The schematic diagram of single-frequency dual polarizations is illustrated in the LR configuration. Figure A represents the retrieval algorithm for LR polarization, while the corresponding algorithm for RR polarization is depicted in Figure B.

The retrieval flowchart for the first line is presented in Figure 7(A), while that for the second line is displayed in Figure 7(B). In other words, the input layers for the different retrieval algorithms vary, and detailed information is provided in the following Table II. The table illustrates that as the input layers for training vary, the retrieval accuracy differs significantly. When surface roughness information and vegetation parameters are included in the training process, the root mean square error (RMSE) decreases. If only the surface reflectivity of LR polarizations is used for training, the RMSE is 0.0700 (compared to 0.0681 for RR polarization, which is slightly better than using only LR polarization). However, when all the parameters mentioned above are employed, the retrieval accuracy (RMSE) for both polarizations can be as good as approximately 0.03.

B. Dual Polarization Retrieval

From the development of space-borne GNSS-R payloads, it is obvious that the properties of polarization for the surface reflected signals must be considered. With the theory equations, we simulate the properties of Fresnel reflectivity(square), bare soil surface reflectivity and the total surface reflectivity. The detail information is provided in the following figure.

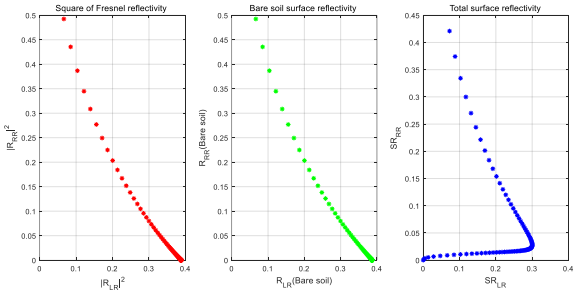

Fig. 8. relationship between the surface reflectivity of LR and RR polarizations. (a) square of Fresnel reflectivity; (b) bare soil surface reflectivity; (c) total surface reflectivity.

Fig. 8. illustrates the relationship between the surface reflectivity of LR and RR polarizations. It is evident that for Fresnel reflectivity and bare soil conditions, the surface reflectivity of LR and RR polarizations is nearly identical. However, when vegetation is factored in, their relationship undergoes a significant change compared to the previous scenarios. In the subsequent study, we will incorporate the theoretical simulations mentioned above.

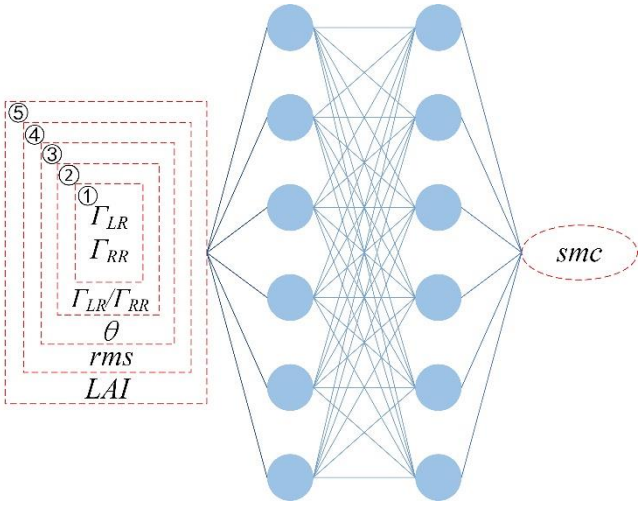

Fig. 9. the retrieval schematic for dual polarization.

Fig. 9. demonstrates the retrieval results for four cases utilizing two polarizations. In the first case, only the surface reflectivity of LR polarization and RR polarization are taken into consideration, while the ratio of surface reflectivity for the two polarizations is considered for the second case. The root mean square error (RMSE) has not improved, with RMSE for Case 1 and Case 2 being 0.0695 and 0.0731, respectively. In the third case, as mentioned in our simulations, the observation geometry (incidence angles) is considered for the final retrieval, resulting in an improved retrieval accuracy with an RMSE of 0.0710. However, when the surface roughness (rms height) and vegetation parameters (LAI) are considered, their retrieval accuracy, as presented by RMSE, is 0.0556 and 0.0344, respectively. The detail in formation for the soil moisture retrieval results are demonstrated in Figure 10 and the final

retrieval accuracy was provided in Table II.

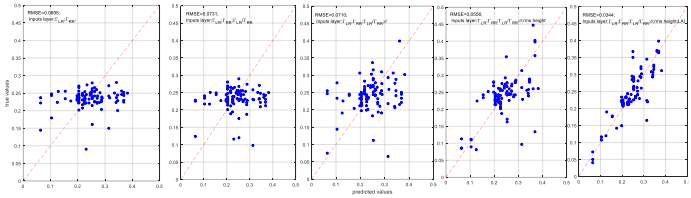

Fig. 10. The retrieval results for dual polarization with different training layer inputs are depicted in the subfigures' captions.

TABLE II RETRIEVAL ALGORITHMS FOR SINGLE POLARIZATION AND DUAL POLARIZATION, INCLUDING THE TRAINING LAYER INPUTS AND THE RETRIEVAL ACCURACY PRESENTED BY RMSE.

Polarization	Case No.	Training layers	RMSE
LR polarization	Case 1	SR_{LR}	0.0700
	Case 2	SR_{LR};θ	0.0650
	Case 3	SR_{LR};θ;rms	0.0468
	Case 4	SR_{LR};θ;rms;LAI	0.0320
RR polarization	Case 1	SR_{RR}	0.0681
	Case 2	SR_{RR};θ	0.0650
	Case 3	SR_{RR};θ;rms	0.0402
	Case 4	SR_{RR};θ;rms;LAI	0.0342
Dual polarizations (LR/ RR polarizations)	Case 1	$SR_{LR;}SR_{RR}$	0.0695
	Case 2	$SR_{LR;}SR_{RR;}SR_{LR/}SR_{RR}$	0.0731
	Case 2	$SR_{LR;}SR_{RR;}SR_{LR/}SR_{RR;}$θ	0.0710
	Case 3	$SR_{LR;}SR_{RR;}SR_{LR/}SR_{RR;}$θ;rms	0.0556
	Case 4	$SR_{LR;}SR_{RR;}SR_{LR/}SR_{RR;}$θ;rms;LAI	0.0344

IV. DISCUSSIONS

Although most of the present works related to soil moisture with GNSS-R techniques believed that the coherent scattering (that is the Surface reflectivity) dominate the GNSS-R scattering on land surface, noncoherent scattering properties have also gained increased interest in recent years for retrieval study. While GLORI is the first publicly available aireboren dual polarization GNSS-R with the record of not only coherent scattering but also noncoherent scattering[38], [39]. Here the corresponding information will by analyzed in this section. Fig. 10 presents the Histogram of coherent scattering properties for airborne GLORI data, while the corresponding noncoherent scattering properties are shown in Fig. 11.

Fig. 11. Histogram of coherent scattering properties for airborne GLORI data: A) alfafa;B)apple tree; C) maize; D) pear tree; E) wheat. Light colors in each sub figures indicate the LR polarization, while dark colors are the RR polarizations.

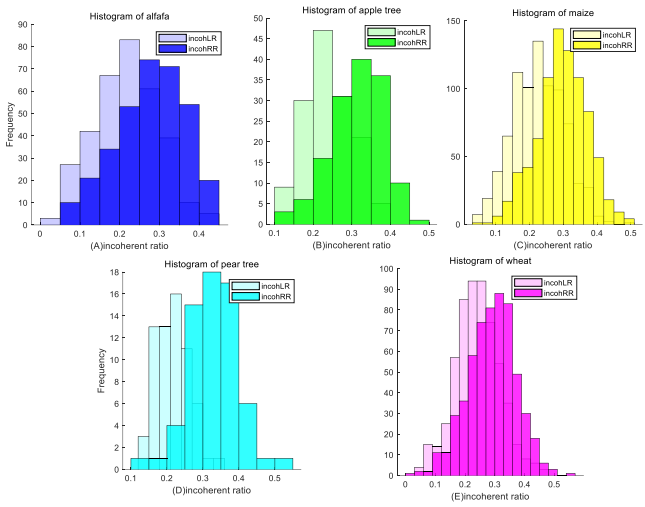

Fig. 12. Histogram of non-coherent scattering properties for airborne GLORI data: A) alfafa;B)apple tree; C) maize; D) pear tree; E) wheat. Light colors in each sub figures indicate the LR polarization, while dark colors are the RR polarizations.

From Figure 11 and Figure 12, we can see that as for coherent scattering, the scattering properties at LR polarization are larger than those at RR polarization. However, this phenomenon is reversed for noncoherent scattering, i.e., the scattering properties at LR polarization are lower than those at RR polarization for the corresponding land surface types.

Utilizing the noncoherent scattering properties of GLORI data, soil moisture retrieval has been conducted, as presented in Table 1. Each case corresponds to a different training layer. "NonCoh" signifies the non-coherent scattering properties, with subscripts "LR" or "RR" indicating their respective polarizations. θ represents the incidence angle, while LAI denotes vegetation information. Root Mean Square Error (RMSE) serves as an indicator of retrieval accuracy. The results reveal that as the input layers for training expand from solely surface reflectivity to include surface roughness and vegetation parameters, the accuracy improves from an initial value of approximately 0.08 to about 0.03.

TABLE III SOIL MOISTURE RETRIEVAL RESULTS WITH NONCOHERENT SCATTERING PROPERTIES . WHILE THE TRAINING LAYERS OF NonCohSR WITH LR OR RR POLARIZATIONS INDICATE THE SURFACE REFLECTIVITY OF NON-COHERENT SCATTERING.

Polarization	Case No.	Training layers	RMSE
NonCoh LR polarization	Case 1	$NonCohSR_{LR}$	0.0821
	Case 2	$NonCohSR_{LR}$;θ	0.0728
	Case 3	$NonCohSR_{LR}$;θ;rms	0.0422
	Case 4	$NonCohSR_{LR}$;θ;rms;LAI	0.0293
RR polarization	Case 1	$NonCohSR_{RR}$	0.0853
	Case 2	$NonCohSR_{RR}$;θ	0.0741
	Case 3	$NonCohSR_{RR}$;θ;rms	0.0569
	Case 4	$NonCohSR_{RR}$;θ;rms;LAI	0.0348
Dual polarizations (LR and RR polarizations)	Case 1	$NonCohSR_{LR;}NonCohSR_{RR}$	0.0832
	Case 2	$NonCohSR_{LR;}NonCohSR_{RR;}$θ	0.0759
	Case 3	$NonCohSR_{LR;}NonCohSR_{RR;}$rms;θ	0.0502
	Case 4	$NonCohSR_{LR;}NonCohSR_{RR;}$rms;θ; LAI	0.0352

Dual Pol(Coh+NonCoh)	Case 1	$CohSR_{LR};CohSR_{RR};NonCohSR_{LR};NonCohSR_{RR}$	0.0823
	Case 2	$CohSR_{LR};CohSR_{RR};NonCohSR_{LR};NonCohSR_{RR};\theta$	0.0764
	Case 3	$CohSR_{LR};CohSR_{RR};NonCohSR_{LR};NonCohSR_{RR};\theta;rms$	0.0518
	Case 4	$CohSR_{LR};CohSR_{RR};NonCohSR_{LR};NonCohSR_{RR};\theta;rms;LAI$	0.0316

Initially, it was believed that the RR polarization of the reflected signals from the Earth's surface was too weak to be received. Therefore, LHCP polarizations of the antenna were employed and designed to isolate the direct signals of the GNSS constellation, whose signals were RHCP polarized, to reduce the effects of multipath signals. Meanwhile, the reflected signals from the Earth's surface were assumed to be from specular points, and the non-coherent scattering information was ignored. However, with the analysis of GLORI experiment data in this paper, we can observe that the reflected signals of RR polarization were indeed weaker than those of LR polarization. Nevertheless, they can be received. With the data of RR polarization and dual polarization (LR and RR), we carried out retrieval algorithms. The results showed that the retrieval accuracy with RR and dual polarization (LR and RR) was comparable to that of single polarization (LR polarization).This finding is significant for the future design of GNSS-R payloads. It suggests that the consideration of RR polarization, and potentially other polarizations, can improve the performance of GNSS-R soil moisture retrieval.

The retrieval with the non-coherent scattering properties also indicates that the non-coherent scattering energy should not be ignored. It should be received and utilized for soil moisture retrieval. The retrieval accuracy with the consideration of both coherent specular scattering and non-coherent scattering, which is recorded as the ratio of non-coherent scattering to total scattering energy, was comparable to that of algorithms that only considered specular scattering.These analysis results indicate that the scattering energy of non-coherent scattering should not be ignored in GNSS-R soil moisture retrieval. Future space-borne GNSS-R payloads should take this information into consideration.

With the increasing availability of polarization and scattering energy information, the hardware of GNSS-R payloads should be improved. This opens up new research avenues, and the corresponding retrieval algorithms are also suitable for deep learning approaches.

V. Conclusion

In recent years, the field of GNSS-R (Global Navigation Satellite System Reflectometry) has witnessed substantial progress, with a particular emphasis on polarization. Initially overlooked in GNSS-R research, polarization has now emerged as a critical area of exploration. Researchers are increasingly recognizing the potential of polarization to enhance the precision and accuracy of remote sensing measurements.

The application of dual polarization for single-frequency data, as demonstrated by airborne experiments such as GLORI, has opened up new avenues for investigation. Theoretical analyses have laid the groundwork for the development of sophisticated retrieval algorithms, leading to improved soil moisture estimation capabilities. By incorporating additional surface parameters, including surface roughness and vegetation characteristics, researchers have observed a significant improvement in retrieval accuracy, as indicated by reduced RMSE (Root Mean Square Error) values.

Furthermore, comparative analyses of the retrieval accuracies between LR (Left-Right) and RR (Right-Right) polarizations have yielded promising results, suggesting potential for further refinement. Notably, the exploration of dual polarizations (LR and RR) has shown retrieval accuracies comparable to those achieved using a single polarization approach. This suggests that the consideration of dual polarization, in conjunction with factors such as surface roughness, LAI (Leaf Area Index), and incidence angle, holds significant promise for advancing soil moisture estimation within the GNSS-R framework.

These advancements underscore the growing importance of polarization in GNSS-R studies and point towards a promising future trajectory for research and practical applications.

Acknowledgment

This research was funded by the National Natural Science Foundation of China (No. 42061057).and Key Laboratory of Satellite Navigation Technology

References

[1] Hall, D., & Cordey, R. A., "Multistatic scatterometry," *IEEE International Geoscience and Remote Sensing Symposium*, 1988, pp.561-562.

[2] Martin-Neira, M., "A Passive Reflectometry and Interferometry System (PARIS)-Application to ocean altimetry," ESA Journal, ESA headquarters, 1993, pp. 331-355.

[3] V., U.Z., et al., "Tutorial on Remote Sensing Using GNSS Bistatic Radar of Opportunity," *IEEE Geoscience and Remote Sensing Magazine*, 2(4), pp.8-45, 2014.

[4] Cardellach, E., et al., "GNSS-R ground-based and airborne campaigns for ocean, land, ice, and snow techniques: Application to the GOLD-RTR data sets," *Radio Science*, 46(null), RS0C04, 2011.

[5] Camps, A., et al., "Review of GNSS-R instruments and tools developed at the Universitat Politecnica de Catalunya-Barcelona tech. in Geoscience and Remote Sensing Symposium",2014.

[6] Gleason, S., Adjrad, M., & Unwin, M., "Sensing Ocean, Ice and Land Reflected Signals from Space: Results from the UK-DMC GPS Reflectometry Experiment," In The 18th International Technical Meeting of the Satellite Division of The Institute of Navigation, Long Beach, CA, USA.2005.

[7] Li, W. Q., Cardellach, E., Fabra, F., et al., "First Spaceborne Phase Altimetry over Sea Ice Using TechDemoSat-1 GNSS-R Signals," *Geophysical Research Letters*, 44(16), pp.8369-8376, 2017.

[8] Rodriguez-Alvarez, N., Holt, B., Jaruwatanadilok, S., et al., "An Arctic Sea Ice Multi-step Classification Based on GNSS-R Data from the TDS-1 Mission," *Remote Sensing of Environment*, 230, 111202, 2019.

[9] Ruf, C. S., et al., "The CYGNSS nanosatellite constellation hurricane mission," *Geoscience and Remote Sensing Symposium*, 2012.

[10] Chew, C. C., & Small, E. E., "Soil moisture sensing using spaceborne GNSS reflections: Comparison of CYGNSS reflectivity to SMAP soil moisture," *Geophysical Research Letters*, 2018.

[11] Al-Khaldi, M. M., et al., "Time-Series Retrieval of Soil Moisture Using CYGNSS," *IEEE Transactions on Geoscience & Remote Sensing*, pp.1-10,2019.

[12] High Spatio-Temporal Resolution CYGNSS Soil Moisture Estimates Using Artificial Neural Networks, 2019.

[13] Zhounan, D., “Effects of the surface vegetation and roughness on spaceborne GNSS-R-derived soil moisture,” 2019.

[14] Calabia, A., Molina, I., & Jin, S., “Soil Moisture Content from GNSS Reflectometry Using Dielectric Permittivity from Fresnel Reflection Coefficients,” *Remote Sensing*, 2020.

[15] Yueh, S. H., et al., “A Semiempirical Modeling of Soil Moisture, Vegetation, and Surface Roughness Impact on CYGNSS Reflectometry Data,” *IEEE Transactions on Geoscience and Remote Sensing*, 60, 2022.

[16] Camps, A., et al., “Sensitivity of GNSS-R Spaceborne Observations to Soil Moisture and Vegetation,” *IEEE Journal of Selected Topics in Applied Earth Observations & Remote Sensing*, 9(10), 2016, pp.4730-4742.

[17] Santi, E., et al., “Remote Sensing of Forest Biomass Using GNSS Reflectometry” *IEEE Journal of Selected Topics in Applied Earth Observations and Remote Sensing*, 2020.

[18] Carrenoluengo, H., Luzi, G., & Crosetto, M., “Above-Ground Biomass Retrieval over Tropical Forests: A Novel GNSS-R Approach with CyGNSS,” *Remote Sensing*, 12(9), 1368,2020.

[19] Clara, C., Reager, J. T., & Eric, S., “CYGNSS data map flood inundation during the 2017 Atlantic hurricane season,” *Scientific Reports*, 8(1), 9336,2018.

[20] Loria, E., et al., “Analysis of scattering characteristics from inland bodies of water observed by CYGNSS,” *Remote Sensing of Environment*, 245, 111825,2020.

[21] Derksen, C., et al., “Retrieving landscape freeze/thaw state from Soil Moisture Active Passive (SMAP) radar and radiometer measurements,” *Remote Sensing of Environment*, 194, pp. 48-62, 2017.

[22] H., C., & C., S. R., “Retrieving Freeze/Thaw Surface State From CYGNSS Measurements,” *IEEE Transactions on Geoscience and Remote Sensing*, 60, pp.1-13,2022.

[23] Wu, X. R., Dong, Z. N., Jin, S. G., et al., “First Measurement of Soil Freeze/Thaw Cycles in the Tibetan Plateau Using CYGNSS GNSS-R Data”. *Remote Sensing*, 12(15), 2361,2020.

[24] Chew, C., et al., “SMAP radar receiver measures land surface freeze/thaw state through capture of forward-scattered L-band signals,” *Remote Sensing of Environment*, 198, pp. 333-344, 2017.

[25] Sun, Y., Huang, F., Xia, J., et al., “GNOS-II on Fengyun-3 Satellite Series: Exploration of Multi-GNSS Reflection Signals for Operational Applications,” *Remote Sensing*, 15, 5756, 2023.

[26] A Novel Soil Moisture Retrieval Algorithm for FY-3E GNOS-R Leveraging Multi-Angle Observations.

[27] Wu, X., Ouyang, X., Wu, S., Wang, F., & Duan, Z., “Assessing the Freeze/Thaw States in Arctic Circle Using FengYun-3E GNOS-R: An Initial Demonstration and Analysis,” *IEEE Journal of Selected Topics in Applied Earth Observations and Remote Sensing*, 17, pp.274-281, 2024.

[28] Unwin, M., et al., “An Introduction to the HydroGNSS GNSS Reflectometry Remote Sensing Mission,” *IEEE Journal of Selected Topics in Applied Earth Observations and Remote Sensing*, 2021.

[29] Wu, X., Chen, L., & Shi, J., “Optimization of Random Surface Scattering Models for RR Polarization in SoOp-R/GNSS-R Applications,” *IEEE Journal of Selected Topics in Applied Earth Observations and Remote Sensing*, 17, pp.4890-4898, 2024.

[30] Wu, X., & Shi, J., “Polarization GNSS-Reflectometry: Potential and Possibility,” *2021 IEEE Specialist Meeting on Reflectometry using GNSS and other Signals of Opportunity (GNSS+R)*, Beijing, China, pp.29-31, 2021.

[31] Dassas, K., et al., “Polarimetric instrument Global Navigation Satellite System - Reflectometry airborne data,” *Data in Brief*, 52, 109850, 2024.

[32] Zavorotny, V. U., & Voronovich, A. G., “Scattering of GPS signals from the ocean with wind remote sensing application,” *IEEE Transactions on Geoscience and Remote Sensing*, 38(2), 2000, pp.951-964.

[33] Wu, X.; Jin, S., “ Models and Theoretical Analysis of SoOp Circular Polarization Bistatic Scattering for Random Rough Surface,” *Remote Sens*., 12, pp.1506, 2020. https://doi.org/10.3390/rs12091506.

[34] X. Wu, L. Chen and J. Shi, "Optimization of Random Surface Scattering Models for RR Polarization in SoOp-R/GNSS-R Applications," *IEEE Journal of Selected Topics in Applied Earth Observations and Remote Sensing*, vol. 17, pp. 4890-4898, 2024, doi: 10.1109/JSTARS.2024.3361923.

[35] Wu, X.; Ouyang, X.; Xia, J.; Yan, Z.; Wang, F., “LAGRS-Soil: A Full-Polarization GNSS-Reflectometry Model for Bare Soil Applications in FY-3E GNOS-R Payload,” *Remote Sens.*, 2023, 15, pp.5296. https://doi.org/10.3390/rs15225296

[36] Wu, X., Wang, F., “LAGRS-Veg: a spaceborne vegetation simulator for full polarization GNSS-reflectometry,” *GPS Solut* 27, 107, 2023. https://doi.org/10.1007/s10291-023-01441-5.

[37] Choudhury, B. J., Schmugge, T. J., Chang, A., & Newton, R. W., “Effect of surface roughness on the microwave emission from soils,” *J. Geophys. Res.* 89, pp.5699–5706,1979. https://doi.org/10.1029/jc084ic09p05699.

[38] Dassas, K., et al., “GLORI: Polarimetric instrument Global Navigation Satellite System - Reflectometry airborne data,” *Data in Brief*, 52: pp. 109850, 2024.

[39] M. Z., et al., “Analysis of Polarimetric GNSS-R Airborne Data as a Function of Land Use,” *IEEE Geoscience and Remote Sensing Letters*, 20: pp. 1-5, 2023.

Xuerui Wu received her Ph.D. degree from Dalian Maritime University (2009/09-2012/12) and got the post-doc position at Shanghai Astronomical Observatory (SHAO), Chinese Academy of Sciences (CAS)(2013/01 to 2014/12), while she is currently an associate professor at SHAO. Her research activities are related to GNSS-Reflectometry and Hydrology. She has concentrated on the topic of GNSS-R land surface scattering models since she was a Ph.D. student in 2009.